Title

Cerebral vascular structure in the motor cortex of adult mice is stable and is not altered by voluntary exercise

Journal

Cerebrovascular and Brain Metabolism Reviews, 37(12)

ISSN

1040-8827

Authors

Cudmore, Robert H
Dougherty, Sarah E
Linden, David J

Publication Date

2017-12-01

DOI

10.1177/0271678x16682508

Peer reviewed

Original Article

JCBFM

Journal of Cerebral Blood Flow & Metabolism
2017, Vol. 37(12) 3725–3743

DOI: 10.1177/0271678X16682508
journals.sagepub.com/home/jcbfm
SAGE

Cerebral vascular structure in the motor cortex of adult mice is stable and is not altered by voluntary exercise

Robert H Cudmore, Sarah E Dougherty and David J Linden

Abstract

The cerebral vasculature provides blood flow throughout the brain, and local changes in blood flow are regulated to match the metabolic demands of the active brain regions. This neurovascular coupling is mediated by real-time changes in vessel diameter and depends on the underlying vascular network structure. Neurovascular structure is configured during development by genetic and activity-dependent factors. In adulthood, it can be altered by experiences such as prolonged hypoxia, sensory deprivation and seizure. Here, we have sought to determine whether exercise could alter cerebral vascular structure in the adult mouse. We performed repeated *in vivo* two-photon imaging in the motor cortex of adult transgenic mice expressing membrane-anchored green fluorescent protein in endothelial cells (tyrosine endothelial kinase 2 receptor (Tie2)-Cre:mTmG). This strategy allows for high-resolution imaging of the vessel walls throughout the lifespan. Vascular structure, as measured by capillary branch point number and position, segment diameter and length remained stable over a time scale of months as did pericyte number and position. Furthermore, we compared the vascular structure before, during, and after periods of voluntary wheel running and found no alterations in these same parameters. In both running and control mice, we observed a low rate of capillary segment subtraction. Interestingly, these rare subtraction events preferentially remove short vascular loops.

Keywords

Cortical plasticity, exercise, pericyte, vascular pruning, vasculature

Received 1 June 2016; Revised 24 October 2016; Accepted 30 October 2016

Introduction

Activated brain regions subserving experience and behavior have a substantial energy demand.[1,2] The cerebral vasculature provides activated brain regions with oxygen and glucose by coupling neural activation to local changes in blood flow, a process called neurovascular coupling.[3,4] Neurovascular coupling is mediated, in part, by the real-time dilation and constriction of blood vessels and is the basis for the blood-oxygen-level dependent signal measured in functional magnetic resonance imaging.[5,6] While chemical signals from neurons and glial cells can modulate cerebral blood flow through local vascular dilation and constriction, the spatial and temporal control of blood flow is ultimately constrained by the underlying cerebral vascular network structure.[7] This network structure includes the overall network topology, the distribution of pericytes, and the properties of individual capillary segments such as diameter, length, and tortuosity.

Vascular network structure is initially configured during embryonic development following some of the same molecular cues that guide axon outgrowth.[8,9] In early postnatal life, experiences such as prolonged hypoxia, sensory deprivation, and seizure can further sculpt vascular networks by promoting both angiogenesis and vessel regression.[10–15] For example, in the whisker barrel cortex of the young mouse, sensory deprivation can reduce and sensory enhancement can increase vascular

The Solomon H. Snyder Department of Neuroscience, The Johns Hopkins University School of Medicine, Baltimore, MD, USA

Corresponding author:
David J Linden, The Solomon H. Snyder Department of Neuroscience, The Johns Hopkins University School of Medicine, 916 Hunterian Building, 725 North Wolfe Street, Baltimore, MD 21205, USA.
Email: dlinden@jhmi.edu

density.[13] Yet, in adulthood, seizures or prolonged hypoxia produce little to no change in vascular structure, indicating that there may be an early critical window for experience-driven vascular plasticity.[11,14,16]

But what about more ethological experiences like exercise? The effects of exercise on brain vasculature have been examined primarily in fixed tissue population studies.[17,18] These reports have shown that exercise can increase vascular capillary density across neocortical, cerebellar, and hippocampal regions of rodents.[19–24] However, these experiments are single time-point studies and so could be missing important processes such as ongoing vessel dynamics within individual animals before and after periods of exercise. They also have reduced statistical power compared to longitudinal measurements within the same animals.

Here, we have examined the long-term cerebral vascular structure in the motor cortex of adult mice and have investigated how this structure changes in response to voluntary exercise. We have chosen to examine the effects of exercise in the motor cortex because motor cortical neurons are robustly engaged during movement[17,25] and there have been claims from fixed-tissue studies that the vasculature of the motor cortex undergoes exercise-dependent plasticity.[21,22]

Some *in vivo* imaging studies examining cerebral vascular structure have used Tie2-green fluorescent protein (GFP) transgenic mice which, due to a limited time-window of GFP expression, only permit endothelial cell imaging in the first few postnatal months.[26] Others have visualized a fluorophore injected into the blood,[27,28] which is an indirect measure of vascular structure and requires repeated intravenous injections. To circumvent these limitations, we have devised a genetic strategy using a Cre-reporter line (Tie2-Cre:mTmG) in which endothelial cells express membrane-anchored GFP under the control of the endothelial cell-specific promoter Tie2.[29] These mice permit repeated and direct visualization of cerebral vascular structure at sub-micron scale across the lifespan of the mouse.

Using this genetic strategy coupled with three-dimensional (3D) image analysis, we performed time-lapse *in vivo* two-photon imaging and measured structural parameters of individual capillary segments, vascular network topology, capillary segment turnover, and pericyte dynamics within layer I and layer II/III of the motor cortex. We then examined the effect of voluntary exercise on cerebral vascular structure by comparing these parameters in individual mice, before, during, and after home-cage wheel running.

Understanding cerebral vascular plasticity following exercise is important because of the wide-ranging beneficial effects of voluntary exercise, which include alleviating anxiety and depression,[30] slowing age-related cognitive decline,[31,32] and speeding recovery from stroke.[33]

Materials and methods

Animals

All experiments were performed in accordance with the National Institutes of Health guidelines and were approved by the Animal Care and Use Committee of The Johns Hopkins University School of Medicine. All animals were housed on a 12-/12-h light–dark cycle, given unlimited access to food and water, and were monitored twice daily for health status. No adverse events were observed. At the end of the experiment, mice were euthanized by deeply anesthetizing with isoflurane (5%, 5 min), cervical dislocation was performed and respiratory arrest was confirmed. All sections of this report adhere to the ARRIVE Guidelines for reporting animal research. A completed ARRIVE guidelines checklist is included in Checklist S1.

Transgenic Tie2-Cre mice (Jackson Labs, Stock Number 008863) were bred with $Rosa^{mT/mG}$ mice (Jackson Labs, Stock Number 007576) and the resultant progeny (Tie2-Cre:mTmG) were used for all experiments. A total of 13 Tie2-Cre:mTmG mice (7 male) were used for *in vivo* imaging (see online supplementary Table 1). At the time of cranial window surgery, 11 of these mice were young adult (122.1 pnd $\pm$ 29.8 SD, median 102) and 2 mice were aged (449 and 681 pnd). Because we did not find differences between male and female mice or mice of different ages, all mice were pooled for analysis.

Home-cage wheel running

In experiments examining the vascular effects of exercise, a random selection of single-housed mice were given unlimited access to a low-profile running wheel (Med Associates) in the home cage. These wireless wheels continuously transmit time-stamped turns and can be locked and unlocked by the experimenter. Mice will run voluntarily when given a home-cage wheel without any additional training or cues. There are differences between animals in both the delay to start running and the total distance run per day. Once running begins, running occurs primarily during the dark-phase of a 12 -/12-h light–dark cycle and the distance run per day increases until it plateaus after one to two weeks. This increase in the distance run is presumably due to a combination of motor learning and improved fitness. For a subset of mice, we obtained both control (no running) and running data (see online supplementary Table 1).

Data analysis

Image stacks were analyzed in Igor Pro (Wavemetrics) using custom software (see http://robertcudmore.org).

All analyses were performed in 3D on unprocessed image stacks. Analysis was performed blind to the experimental condition and the interval between imaging sessions. For images presented in figures, contrast was adjusted for clarity.

Statistical analysis

Statistical analysis was performed in Igor Pro (Wavemetrics) and R (version 3.3.0, www.R-project.org). Sample sizes were chosen according to previously published literature.[11,13,14] Statistical significance was calculated using the non-parametric Wilcoxon signed-rank test for paired comparisons (Figures 2(a) and (b), 3(a) to (d)), the non-parametric Mann–Whitney test for un-paired comparison (Figure 6(b) and (c)), one-way analysis of variance with post hoc Bonferroni correction (Figure 2(d)), and a likelihood ratio test for generalized linear models (GLMs, Figures 4(b) and (c), 5(b) and (c)). All data are presented as mean ± standard error of the mean (SEM) unless otherwise noted.

Results

In vivo imaging of cerebral vasculature in Tie2-Cre:mTmG mice

To visualize the long-term structural dynamics of cerebral vasculature, we crossed a Cre reporter mouse (mTmG)[34] with a transgenic mouse in which the expression of Cre recombinase is driven by the endothelial cell-specific promoter Tie2 (Tie2-Cre).[29] The resultant cross (Tie2-Cre:mTmG) has endothelial cells, pericytes, and some microglia (data not shown) labeled with membrane-anchored GFP and all other tissue labeled with membrane-anchored tdTomato. This pattern of expression was stable for all ages examined (3–22 months).

By performing *in vivo* two-photon imaging through a cranial window, we can visualize the fine structure of cerebral vasculature from the pial surface to depths of ~500 μm (Figure 1(a), online supplementary Movies 1 and 2). Using the expression of tdTomato, we can discern pial arteries from veins as pial arteries are wrapped by smooth muscle cells and veins are not (online supplementary Figure 3).[35] Neuronal somata can be visualized as tdTomato-lacking black holes. This allows for the easy identification of the boundary between cortical layer I and layer II/III as layer II/III has a higher density of neuronal somata (Figure 1(b); layer II/III transition 142.5 ± 2.0 μm from the pial surface, n = 10 mice). Finally, we are able to visualize pericytes adhering to capillary segments by their characteristic bump-on-a-log morphology throughout layers I and II/III (Figure 1(c)).[35–37] This Tie2-Cre-dependent expression of GFP in pericytes is supported by previous studies which showed that pericyte precursor cells do in fact express the Tie2 receptor.[38,39]

To verify that GFP expressing cells with a 'bump-on-a-log' morphology were in fact pericytes, we performed double antibody staining in fixed-tissue slices from Tie2-Cre:mTmG mice and examined the co-localization of GFP with the pericyte marker CD13.[40] We marked the position of candidate pericytes using the GFP channel and then quantified the number of these candidates that showed co-labeling with CD13 (online supplementary Figure 4). With this strategy, we find that 75% of our GFP^+ candidate pericytes (scored using only the GFP channel) show co-localization with CD13 (n = 518 pericyte candidates in 12 slices from four animals). Within this $GFP^+/CD13^+$ population, 22% (83/386) had full overlap between GFP and CD13 labeling along the protruding membrane. The remaining 78% (303/386) of GFP^+ protrusions had partial overlap of labeling for CD13. When all 386 candidate pericytes were scored together, 0.54 ± 0.23 SD (range of 0.12 to 1.0) of the GFP^+ membrane was co-localized with $CD13^+$ staining.

To determine the population of candidate pericytes that would be missed by scoring only GFP^+ protrusions, we have attempted to exhaustively count the protruding somata using the CD13 channel within the imaging volume. This yielded 176 $CD13^+/GFP^-$ protrusions. Thus, the proportion of $CD13^+/GFP^-$ protrusions was 176/694 = 0.25.

Determining the fraction of candidate pericytes that are indeed pericytes is complicated by several factors. One estimate is 75%, the fraction of GFP^+ protrusions that were also $CD13^+$. However, this number may be an underestimate because $GFP^+/CD13^-$ candidate cells may be pericytes or they may not as it has not been established that anti-CD13 (or any other antibody for that matter) labels every pericyte. On the other hand, some $GFP^+/CD13^+$ protrusions may represent a long pericyte process draped over an endothelial cell soma, thereby contributing to an overestimate of pericyte density.

Because Tie2-Cre:mTmG mice are endowed with GFP expressing endothelial cells, the resultant images are of lamina-labeled hollow tubes. Most currently available tube-tracing software is designed to analyze filled tubes.[41,42] Thus, to quantify our 3D time-lapse *in vivo* images, we developed custom tracing software for hollow tubes to extract vascular parameters including network topology, branch point position, and vessel segment length and diameter (Figure 1(d); online supplementary Figure 1).

By combining these genetic, *in vivo* imaging, and image analysis techniques, we have sought to ask how the adult cerebral vasculature changes with time and in response to voluntary exercise.

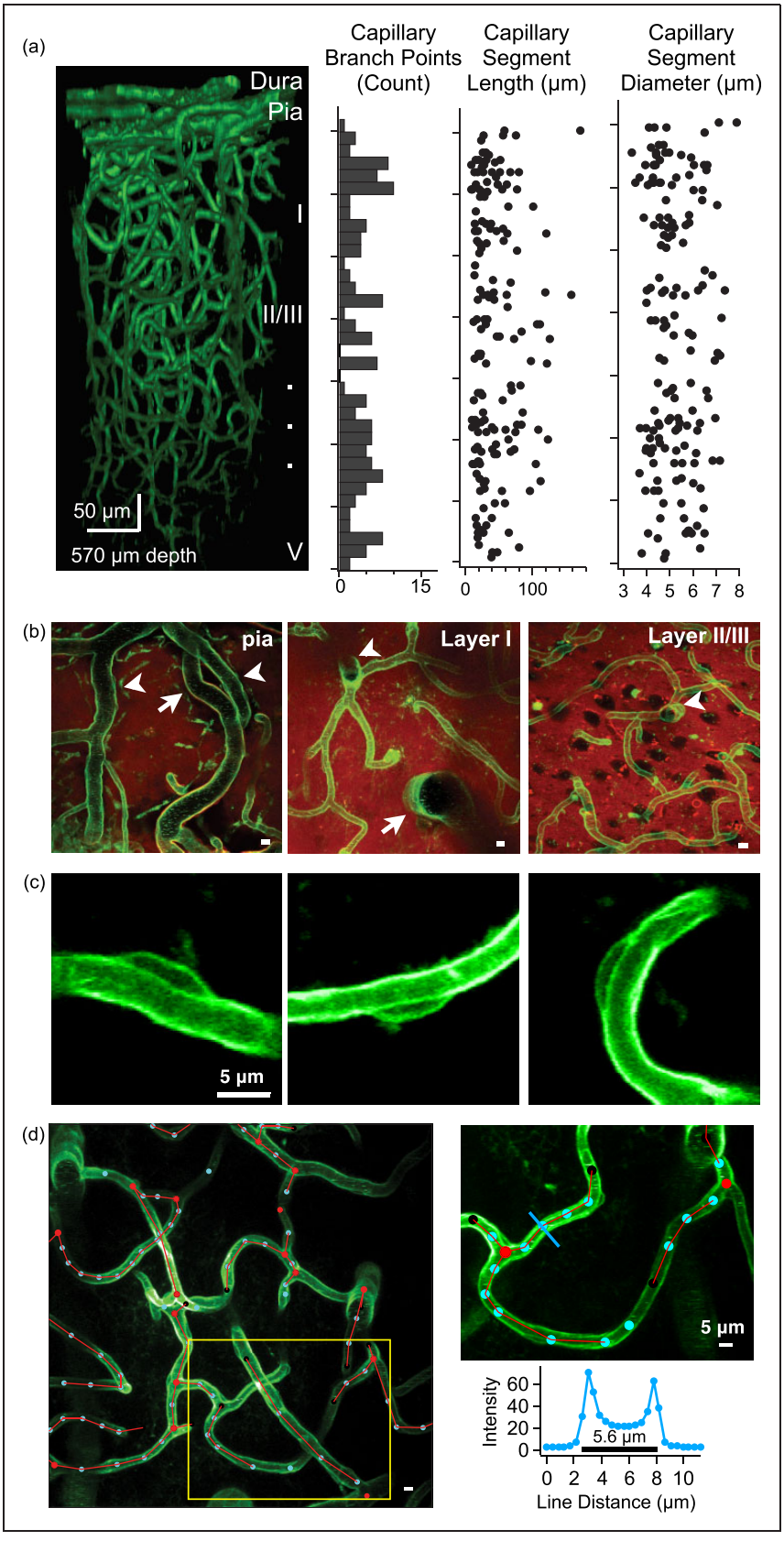

Figure 1. *In vivo* imaging of cerebral vasculature. (a) An exemplar 3D reconstruction of motor cortex vasculature imaged in an adult Tie2-Cre:mTmG mouse (left). Plots illustrate the number of capillary branch points (histogram), capillary segment length, and capillary segment diameter as a function of cortical depth for this same reconstruction. (b) Maximal-intensity projections of imaging planes at the level of the pial surface (left, 12-µm thick projection), layer I (middle, 30 µm projection), and layer II/III (right, 30 µm projection). The pial surface has large arteries (arrow) and veins (arrow heads), layer I is mostly devoid of neuronal somata while layer II/III has a

(continued)

Pericyte distribution on capillary segments

We characterized the distribution of pericytes in layers I and II/III of primary motor cortex. Pericytes are contractile cells that closely associate with epithelial cells and wrap processes around vessels. They are found throughout the vascular network including cerebral capillaries where they help to maintain the blood–brain barrier and control vascular tone.[35,43–49]

Focusing on pericytes associated with capillary segments, we scored two classes based on the position of their cell body including 'en passant pericytes' with their somata positioned along the length of capillary segments and 'junctional pericytes' with their somata at capillary branch points (Figure 2).[35,40,43] Of all capillary-associated pericytes scored, 77% were en passant while the remaining 23% were junctional ($n = 1399$ total pericytes in 10 mice). En passant pericytes occurred on 43% of capillary segments ($n = 2494$ total capillary segments in 10 mice) and junctional pericytes occurred on 13% of branch points ($n = 2449$ total branch points in 10 mice).

We compared the percentage of capillary segments with and without en passant pericytes between layers I and II/III and find that layer I has a significantly higher density of capillary segments possessing a pericyte (Figure 2(a); layer I $45.7 \pm 5.3\%$; layer II//III $33.4 \pm 5.4\%$, $p = 0.002$ in 10 mice). This corresponds to approximately 1.4 and 1.1 pericytes per 100 μm of capillary segment in layer I and II/III, respectively, whereas junctional pericytes had an equal probability of being associated with a branch point in both layers I and II/III (Figure 2(b); layer I $13.7 \pm 1.8\%$; layer II//III $12.0 \pm 1.2\%$, $p = 0.38$ in 10 mice). These results are consistent with a recent report, which assayed the distribution of pericytes using immunohistochemistry in a cleared-brain preparation.[40] The layer-specific heterogeneous distribution of pericytes could reflect functional differences between these capillaries with layer I capillaries providing blood flow primarily to axons, apical dendrites and synapses of pyramidal cells with their cell bodies in deeper cortical layers, and layer II/III capillaries mainly supplying blood to neuronal somata of pyramidal cells with their cell bodies in layers II/III as well as the apical dendrites of pyramidal cells with somata residing in deeper cortical layers.

Given that en passant pericytes only occur on a fraction of capillary segments, we wanted to determine if capillary segments with and without a pericyte represented two different structural classes (Figure 2(c) and (d)). By comparing the length and diameter of capillary segments with and without en passant pericytes, we find that en passant pericytes occur on significantly longer capillary segments (without pericyte 39.9 ± 2.9 μm; with pericyte 69.9 ± 4.6 μm; $p < 0.001$ in 10 mice) and on capillary segments with significantly smaller diameter (without pericyte 6.1 ± 0.1 μm; with pericyte 4.8 ± 0.1 μm; $p < 0.001$ in 10 mice). We occasionally observed more than one (usually two to three) pericyte cell bodies on the longest capillary segments. In general, these pericyte cell bodies were evenly distributed and were not aggregated or clumped. By grouping capillary segments with no pericyte, one pericyte, and greater than one pericyte (Figure 2(d)), we find the number of pericytes on a capillary segment increases with segment length. Furthermore, as pericytes are added to longer capillary segments, there is a monotonic decrease in capillary diameter.

Longer capillary segments tend to have smaller diameters regardless of whether or not they have an associated pericyte. Thus, as a control, we compared the diameter of capillary segments with and without pericytes for a subset of capillary segments with similar lengths (20–40 μm) and found that length-matched capillary segments with a pericyte have a significantly smaller diameter than their counterparts without a pericyte (without pericyte 5.5 ± 0.1 μm; with pericyte 5.07 ± 0.1 μm; $p = 0.004$ in 10 mice).

The presence of a pericyte cell body is proposed to be associated with a constriction of the underlying portion of the vessel to which it adheres.[36] To test this idea, we compared the diameter of individual capillary segments at pericyte cell bodies versus away from pericyte cell bodies but find no significant difference between these two cases (online supplementary Figure 5).

Taken together, these results show that pericytes are preferentially associated with longer capillary segments and those segments possessing a pericyte have a smaller

Figure 1. Continued.
higher density of neuronal somata (which appear as black holes in the red fluorescence channel). Both layer I and II/III have capillary segments, diving arterioles (arrow) and ascending venules (arrow head). Scale bars are 5 μm. (c) Maximal-intensity projections of three pericyte cell bodies adhering to capillary segments in layer II/III. (d) An exemplar image showing semi-automated 3D tracing of vasculature in layer II/III (left) showing branch points (red circles), way-points (blue circles), and red connecting lines. Image is a maximal z-projection from 200 to 220 μm depth from the pial surface, scale bar is 5 μm. The panel in the upper right shows a detailed view of the capillary segment tracing which corresponds to the yellow box on the left image. The blue line is used to measure capillary diameter at one way point, using the intensity profile (lower right).

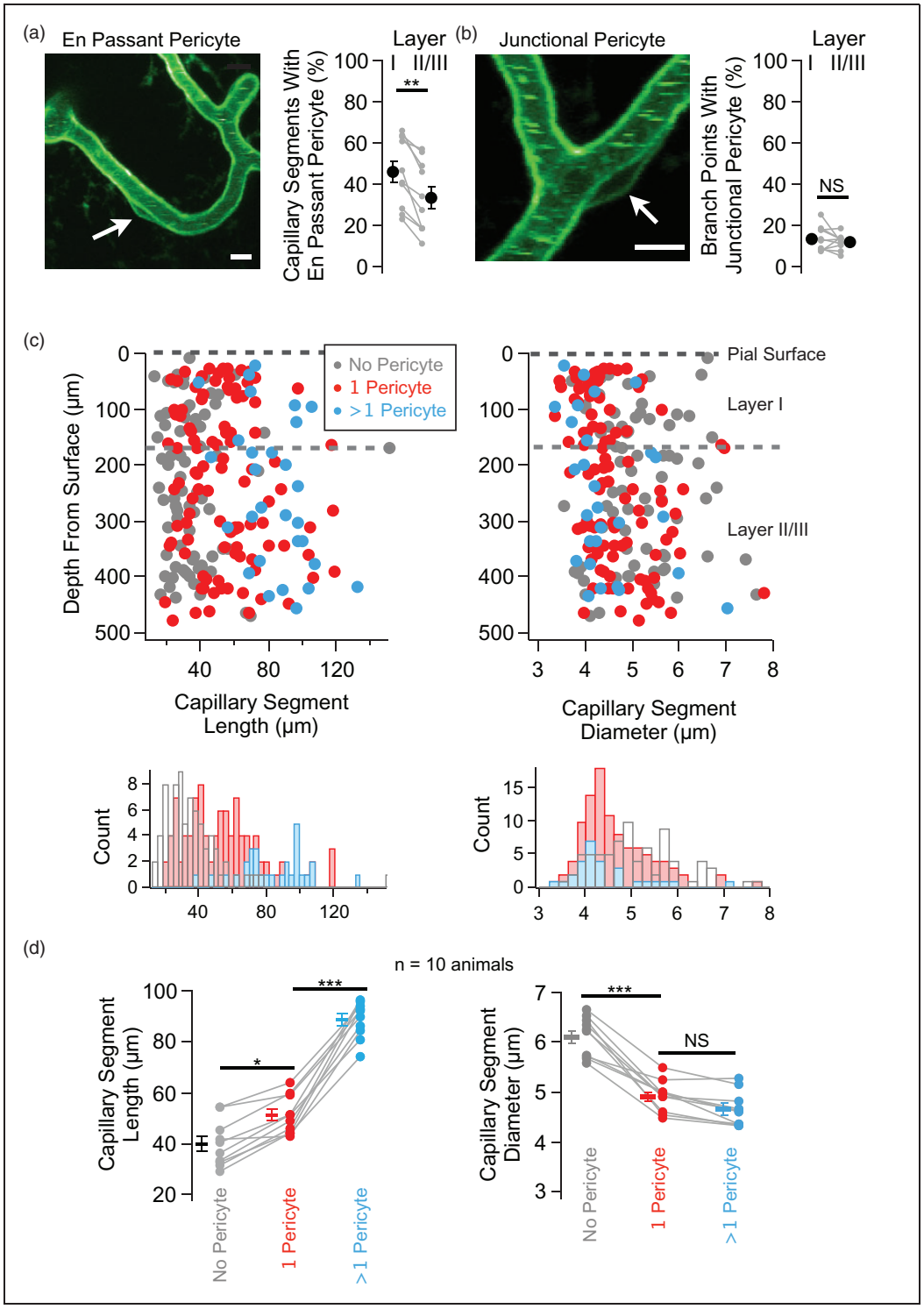

Figure 2. Pericyte distribution on capillary segments. (a) Exemplar image of an en passant pericyte (left) and group data of the percentage of capillary segments in layer I versus layer II/III that possess an en passant pericyte (n = 10 mice, $^{**}p < 0.01$, Wilcoxon signed-rank test). (b) Exemplar image of a junctional pericyte (left) and group data of the percentage of branch points in layer I versus layer II/III that possess a junctional pericyte (n = 10 mice, NS indicates not significant, p = 0.375, Wilcoxon signed-rank test). (c) Capillary segment length and diameter plotted as a function of depth from the brain surface for capillary segments with different numbers of en passant pericyte cell bodies (no pericyte, gray, n = 77; 1 pericyte, red, n = 101; > 1 pericyte, blue, n = 30; data are from one animal). The black-dotted line represents the pial surface and the gray-dotted line shows the transition between layer I and layer II/III. The histograms show the distribution of capillary segment length (left) and diameter (right) for capillaries with no pericytes (gray),

(continued)

average diameter compared to their pericyte-free counterparts, but that this constriction is not precisely localized to the portion of the vessel underlying the pericyte cell body.

Isoflurane anesthetic dilates cerebral vessels

We began examining the long-term structural plasticity of cerebral vasculature by repeatedly imaging mice anesthetized with isoflurane anesthetic. Isoflurane is known to dilate cortical vessels[50–53] and increase capillary Po_2.[54] During our repeated imaging with 1.5% isoflurane, there were significant differences in capillary segment diameter between imaging sessions with one to four day intervals and even within single imaging sessions of less than 1 h. We also found that mice anesthetized with isoflurane had disruptions in the daily distance of home-cage wheel running (data not shown).

To understand the acute effect of isoflurane, we compared the structure of individual vessels during wakefulness and under isoflurane anesthetic. Isoflurane anesthetic dilates all vessels in superficial motor cortex including pial arteries and veins (Figure 3(a)) as well as layer I and layer II/III capillary segments (Figure 3(b)). The dilatory response of isoflurane is not specific to a particular vessel type (Figure 3(c)). By contrast, isoflurane does not change the length of capillary segments (Figure 3(d)).

Given that most vessel segments are dilated by isoflurane, one might expect a concomitant increase in brain volume. Yet, by examining the position of 3D branch points in the awake versus anesthetized we see they are spatially stable (Figure 3(e)). To quantify this, we compared the volume of the 3D convex hull enclosing these capillary branch points and find no difference in the anesthetized versus awake state (awake volume $5.2 \times 10^6 \mu m^3 \pm 1.4 \times 10^6$ versus anesthetized volume $5.1 \times 10^6 \mu m^3 \pm 2.2 \times 10^6$; $n = 4$ animals, $p = 0.38$, Wilcoxon signed-rank test).

Next, we determined whether capillary segments with and without pericyte cell bodies would differ in their dilatory response to isoflurane. We find there is no difference in the absolute change in the diameter of these two classes of capillary segments (with pericyte $0.42 \pm 0.07 \mu m$, $n = 46$ segments; without pericyte 0.51 ± 0.06, $n = 72$ segments; $p = 0.45$ in three mice). Because isoflurane dilates cortical vessels and interferes with subsequent home-cage wheel running, we performed awake head-fixed imaging for the remainder of our experiments.

Cortical vascular structure is stable in the adult

To determine if there are ongoing structural variations in individual vessels, we repeatedly imaged adult Tie2-Cre:mTmG mice and looked for changes in vessel structure including diameter, length, and branch point position. Repeated imaging of the same brain region reveals that the brain vascular structure is remarkably stable (Figure 4(a)). By tracking the diameter and length of individual capillary segments, we find no significant change over a time-span of one month (Figure 4(b)). For this longitudinal analysis, a pseudo-random subset of all capillary segments were traced (see online supplementary methods). By comparing time-points spanning approximately one month (30.4 days $\pm$ 3.3, $n = 8$ animals), we find there is no long-term change in either capillary segment diameter or length (Figure 4(c)). Likewise, the 3D position of capillary branch points is stable (Figure 4(d)) indicating that the volume occupied by brain capillaries remains unchanged. To quantify this, we compared the volume of the 3D convex hull enclosing capillary branch points and find no significant difference over a month interval (initial volume $5.5 \times 10^6 \mu m^3 \pm 1.2 \times 10^6$ versus one-month volume $4.8 \times 10^6 \mu m^3 \pm 1.3 \times 10^6$, $n = 8$ animals, $p = 0.25$, Wilcoxon signed-rank test).

We performed additional analysis looking for layer-specific changes in length and diameter by grouping capillary segments into layer I versus layer II/III and still see no significant changes in either capillary segment diameter or length over a one-month interval (data not shown).

Home-cage wheel running does not effect cortical vascular structure

We have sought to measure the effect of exercise of cerebral vascular structure. We hypothesized that exercise would induce plasticity in vessel structure, by modifying the tone of vessel segments (dilation or constriction), vessel segment length or branch point position or by

Figure 2. Continued.
with one pericyte (red), and with > 1 pericyte (blue). (d) Group data ($n = 10$ mice) showing capillary segment length (left, $^*p = 0.012$, $^{***}p < 0.001$) and diameter (right, $^{***}p < 0.001$, NS indicates not significant, $p = 0.34$) with no pericyte cell body (gray, 506 total segments), with 1 pericyte cell body (red, 421 total segments), and with > 1 pericyte cell body (blue, 136 total segments). Gray lines connect measurements within individual animals and isolated symbols are the group mean $\pm$ SEM. Statistical significance was determined by one-way ANOVA with Bonferroni post hoc correction.

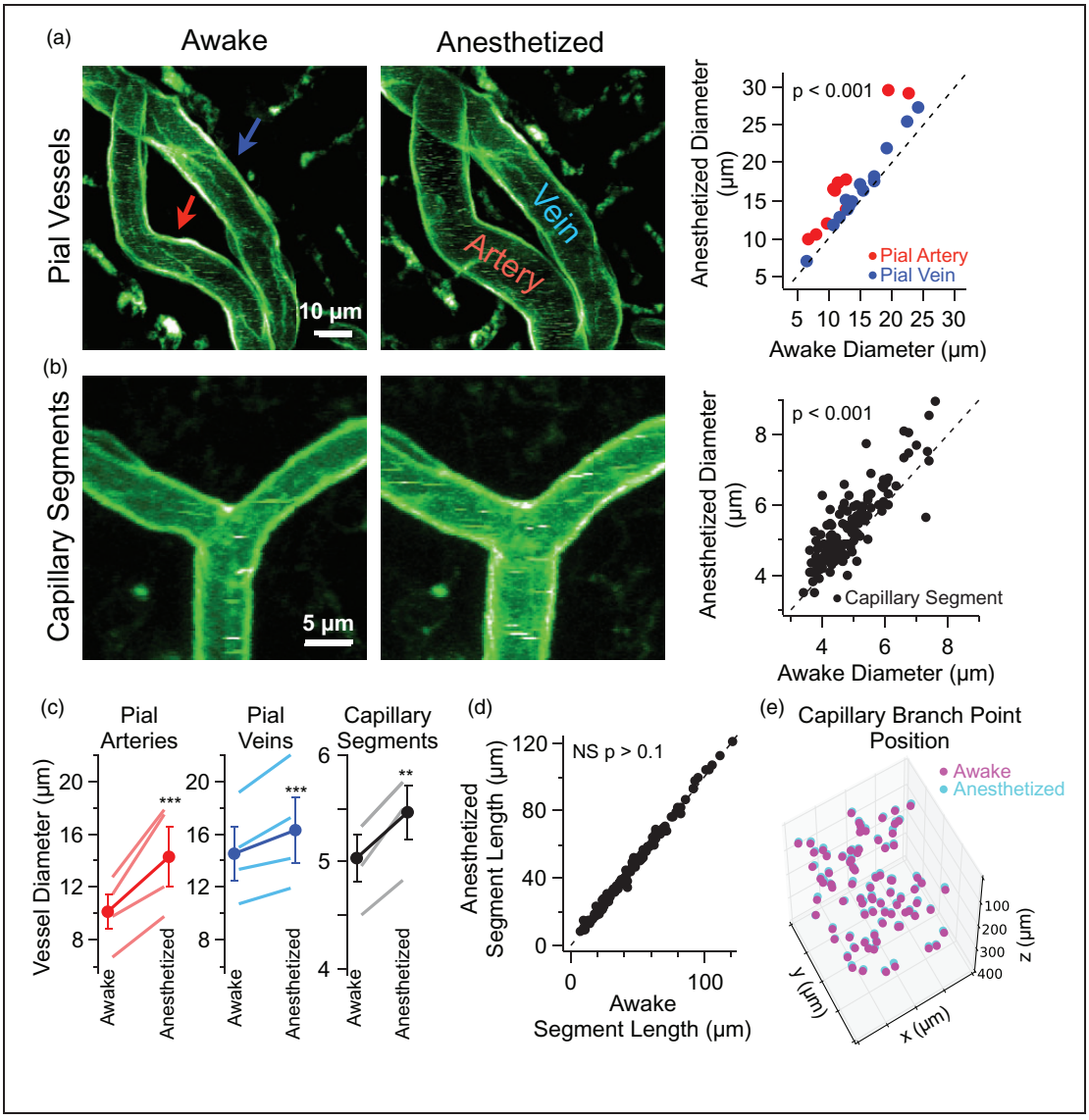

Figure 3. Isoflurane anesthetic dilates all types of blood vessel in the motor cortex. (a) Time-lapse maximal-intensity projections of pial vessels acquired when a mouse was awake (left) and subsequently anesthetized with 1.5% isoflurane (middle). Each image contains the same pial artery (red arrow) and vein (blue arrow). Images were acquired 12–15 min apart. Group data showing the diameter of individual pial arteries and veins in anesthetized versus awake conditions (right, 11 arteries and 14 veins in four mice, $p < 0.001$, Wilcoxon signed-rank test). (b) Time-lapse maximal-intensity projections of capillary segments in layer II/III when the mouse was awake (left) versus anesthetized (middle). Group data showing the diameter of individual capillary segments in anesthetized versus awake (right, $n = 176$ capillary segments in four mice, $p < 0.001$, Wilcoxon signed-rank test). (c) Group data showing changes in the diameter of pial arteries, pial veins, and capillary segments in awake versus anesthetized conditions. Lines with no symbols represent the mean in individual animals and lines with circle symbol represent the mean ± SEM across animals ($n = 4$ animals, ***$p < 0.001$, **$p = 0.002$, Wilcoxon signed-rank test). Please note that the gray line representing the capillary segment measurements for one animal is obscured by the line for the group mean (right panel). (d) Group data of capillary segment length in awake and anesthetized conditions ($n = 176$ capillary segments in four mice, NS indicates not significant, $p > 0.1$, Wilcoxon signed-rank test). (e) Time-lapse plot of 3D capillary branch point positions in awake (magenta) versus anesthetized (cyan) conditions ($n = 86$ branch points in one mouse). All visible capillary branch points were scored and the boundaries of the image volume are given by the limits of the x, y, and z axis.

adding new vessels or subtracting existing ones. Exercise-induced plasticity in vascular structure could match exercise-induced changes in the metabolic demands of the underlying brain parenchyma.

Mice will spontaneously run in their home-cage when given unlimited access to a running wheel. To quantify home-cage wheel running, we continuously recorded the number of wheel turns and looked for

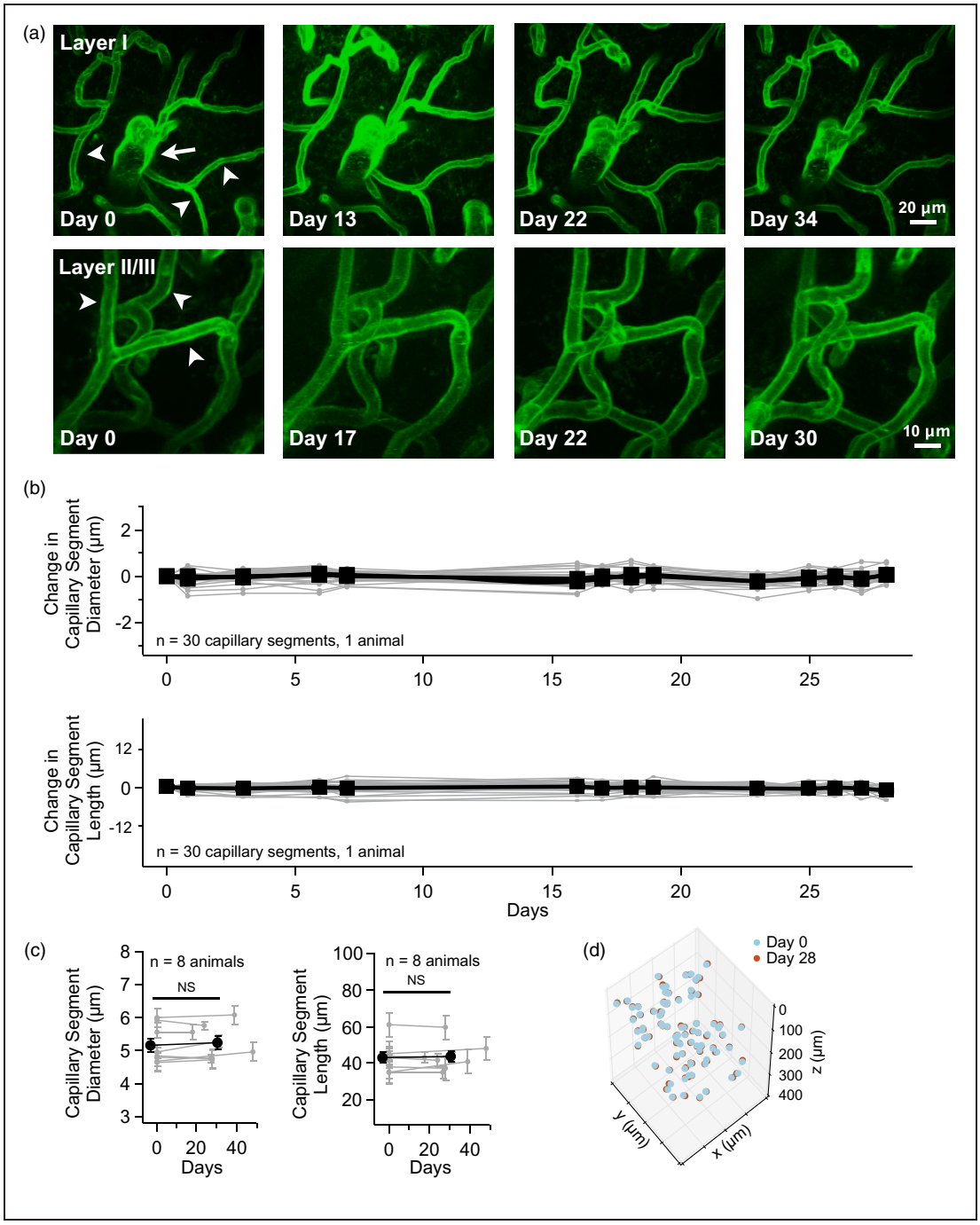

Figure 4. Time-lapse imaging reveals that cerebral vascular structure is stable. (a) Exemplar time-lapse maximal-intensity projections of motor cortex vasculature in layer I (top row) and layer II/III (bottom row). An ascending venule (white arrow) and multiple capillary segments (white arrow heads) are indicated in the first time-point. Please note that these exemplar images are a small portion of the total image volume. (b) Time-course of the change in capillary segment diameter and length over 28 days, with values normalized to day 0 ($n = 30$ capillary segments in one mouse). There was no statistical significance for diameter or length between any of the time-points ($p > 0.1$, $n = 30$ capillary segments in one animal, GLM likelihood ratio test). (c) Group data of the change in capillary segment diameter (left) and length (right) between imaging day 0 and a later time-point (x-axis indicates days). Gray lines connect the mean and gray error bars are SEM within each animal. The number of segments analyzed for each animal was 52.9 ± 38 SD, min/max of 22/118 with median 39 ($n = 8$ animals). The black line with circle marker is grouped mean $\pm$ SEM, $n = 8$ animals, NS indicates not significant, diameter $p = 0.15$, length $p = 0.6$, GLM likelihood ratio test). (d) Time-lapse plot of 3D capillary branch point position. Day 0 (cyan) and day 28 (red) are overlaid to show stability ($n = 83$ branch points in 1 mouse). All visible capillary branch points were scored and the boundaries of the image volume are given by the limits of the x, y, and z axis.

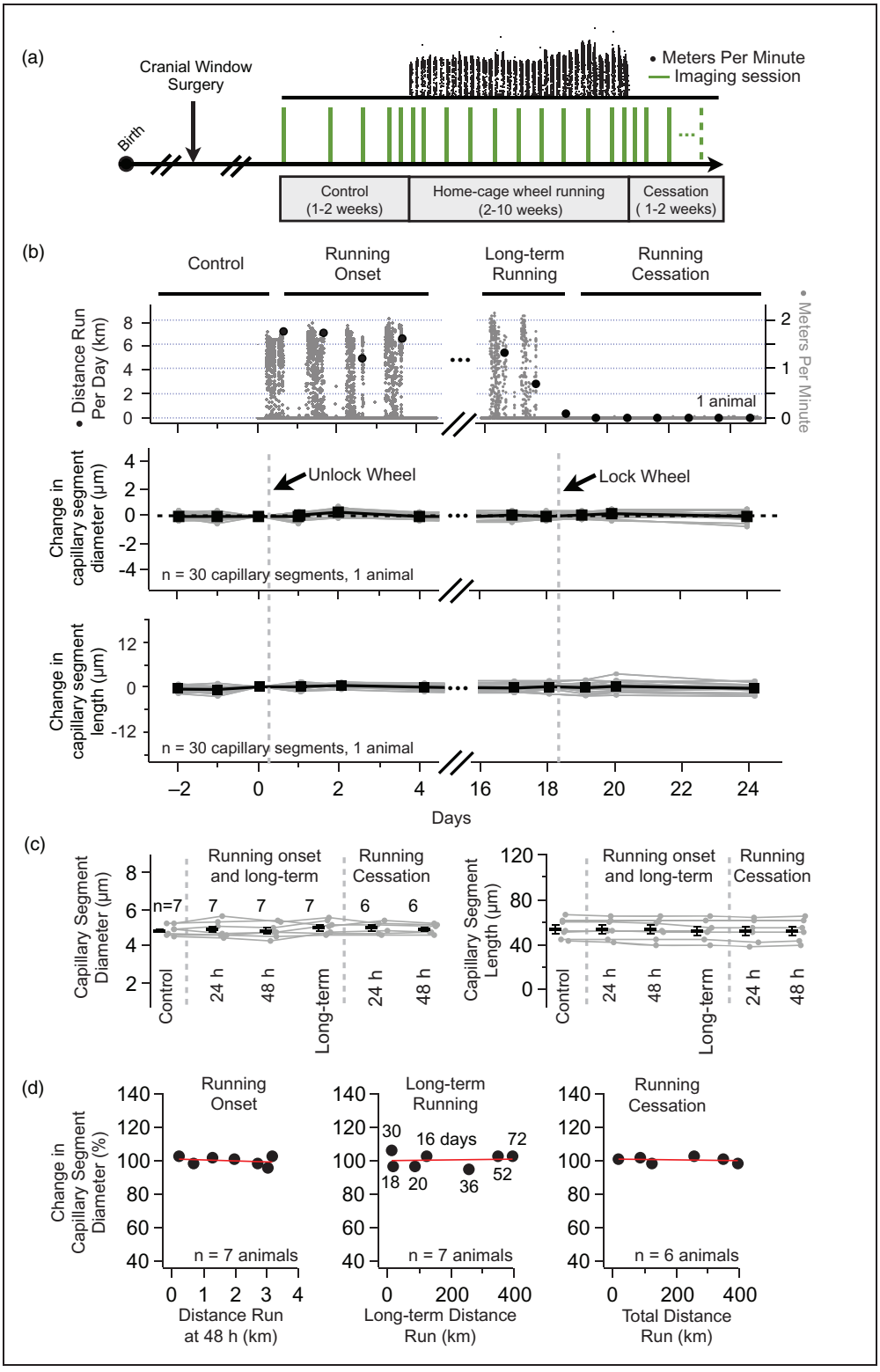

Figure 5. Voluntary wheel running does not alter vascular structure. (a) Experimental design to measure vascular structure before, during, and after home-cage wheel running. Following a cranial window surgery, mice are repeatedly imaged at one- to four-day intervals (vertical green lines). A home-cage running wheel is introduced and the distance run is recorded each minute (top, black dots). Vascular structure is compared in three conditions (control, home-cage wheel running, and running cessation) as well as at the transitions between these conditions (e.g. 24 and 48 h after the start of home-cage wheel running). Control animals were imaged following the same experimental design but did not run on a wheel. (b) Home-cage wheel running and repeated *in vivo* imaging of

correlations between this measure and vascular structural measurements (Figure 5(a)). We compared capillary segment diameter and length (Figure 5(b)) before and after: (i) the onset of running (24/48 h), (ii) during long-term running (2–10 weeks of running), and (iii) after the cessation of running (24/48 h). We do not observe any significant change in the diameter or length of capillary segments in any of these conditions (Figure 5(c)). In addition, the position of capillary segment 3D branch points did not change with exercise (data not shown), indicating that exercise does not produce marked brain expansion or contraction.

We then determined whether the amount of home-cage wheel running correlated with changes in capillary segment structure. By comparing the distance run in each of our three conditions (running onset, long-term running, and running cessation) with the resultant change in capillary segment diameter, we find no correlation (Figure 5(d)). We were especially interested to determine if longer periods of exercise would have an effect on capillary segment diameter. Our hypothesis was that prolonged exercise would result in a general dilation of cortical capillary segments. Yet, we see no significant change in capillary segment diameter after mice run on average 34.9 days $\pm$ 20.7 SD (median 30 days) and for distances of 178.8 km $\pm$ 156.6 SD (median 122 km). Finally, there is no significant difference in the long-term changes of capillary segment diameter between control (Figure 4(c)) and running (Figure 5(c)) animals (% change in control 101.4 ± 1.25 versus running 105.9 ± 1.67, $n = 8$ control animals, $n = 7$ running animals, $p = 0.65$, Mann–Whitney test).

To control for the possibility that the addition of a running-wheel could act as sensory enrichment (independent of exercise), we compared the vascular structure before and after the addition of a locked home-cage running wheel and saw no differences in capillary segment diameter or length accompanying this experience (online supplementary Figure 6).

Taken together, these results show that voluntary exercise does not induce pronounced vascular structural plasticity in layers I–III of the mouse primary motor cortex.

Cortical vasculature undergoes a low rate of capillary subtraction that is not affected by exercise

Recent reports using time-lapse *in vivo* two-photon microscopy have examined ongoing capillary segment dynamics in juvenile versus adult mice (>3 months of age) and find that while adult mice show addition and subtraction of capillary segments, the rate of these events are much less than that observed in juveniles.[11,16]

Here, we searched for capillary segment addition and subtraction in adult mice by exhaustively matching all capillary segments in 3D images acquired approximately three months apart (interval in days 86.7 ± 6.35, median 92; 4973 capillary segments occupying a total volume of 0.24 mm^3 in 11 mice). We did not observe any capillary segment additions but did find a small number of subtractions (Figure 6(a)). In total, we found 42 subtractions, which yield a rate of approximately 0.16 subtractions per day per mm^3.

Next, we determined whether voluntary exercise alters the rate of capillary subtraction compared to control. We see no difference in the rate of capillary subtraction in control versus exercising mice (Figure 6(b); subtractions per day per mm^3 in control 0.16 ± 0.07 versus exercise 0.13 ± 0.07; $p = 0.73$ in 11 mice). For this analysis, we searched for capillary segment addition and subtraction before and after mice exercised for 58.8 days $\pm$ 25.6 SD (median 62 days) and ran on average 192.6 km $\pm$ 159.2 SD (median 131.6 km). One possibility is that exercise could induce transient vessels that were added and then subtracted a few days later.[55] To check this, we compared intermediate imaging time-points during exercise and find no additional additions or subtractions. Finally, we examined imaging sessions

Figure 5. Continued.
vascular structure in an exemplar mouse. The top panel shows a plot of the distance run per minute (gray dots) and the cumulative distance run per day (black circles). The middle and bottom panels are plots of the change in capillary segment diameter and length, normalized to the imaging session before running onset (indicated as "unlock wheel"). Gray symbols connected by gray lines represent repeated measurements for individual capillary segments. Black symbols represent the mean $\pm$ SEM for each time-point. There was no significant change in segment length or diameter in any of the experimental conditions ($p > 0.1$, $n = 30$ capillary segments in one animal, GLM likelihood ratio test). (c) Group data comparing changes in capillary segment diameter (left) and length (right) in control conditions and 24 and 48 h after running onset, after long-term running, and 24 and 48 h after running cessation. Gray symbols connected by gray lines represent the mean $\pm$ SEM at each time-point for individual animals. Black symbols represent the population mean across animals. The number of animals for each condition is indicated in the figure ($n = 6$–7). There was no significant difference between any of the conditions (diameter $p = 0.19$, length $p = 0.2$, GLM likelihood ratio test). (d) Group data comparing the change in capillary segment diameter as a function of the distance run at the onset of wheel-running (left, Pearson's $r = -0.3$, $n = 7$ mice), after 2–10 weeks of running (middle, Pearson's $r = 0.06$, $n = 7$ mice), and after the cessation of running (right, Pearson's $r = -0.23$, $n = 6$ mice). Numbers next to symbols in middle plot indicate the number of days running for each animal. Each plot symbol represents one animal. In all plots, the red line is a linear fit of the plot points.

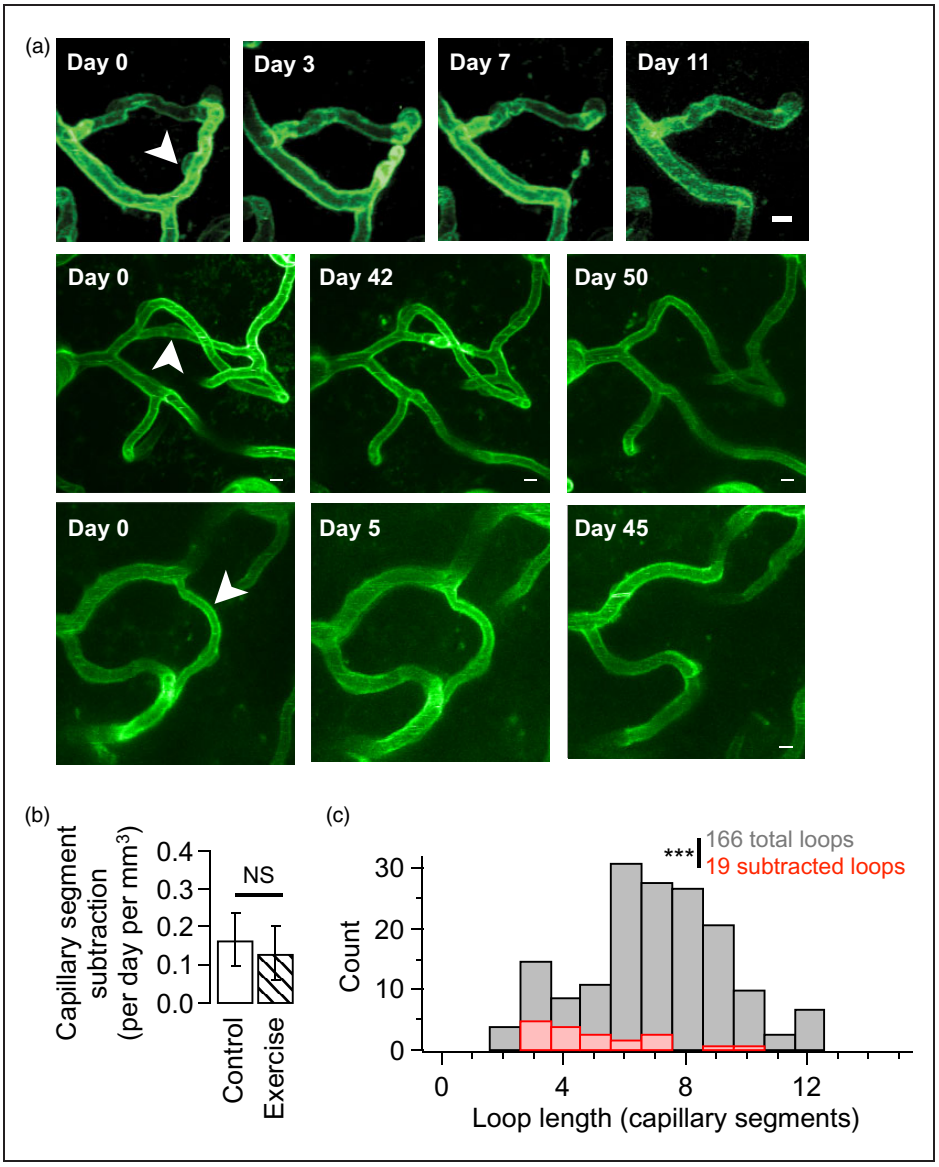

Figure 6. Capillary segment subtractions preferentially prune short vascular loops. (a) Exemplar time-series showing rare capillary segment subtractions. Each row shows a time-lapse series of one capillary segment subtraction (white arrow head). Each image is a maximal-intensity z-projection chosen to illustrate the local vascular topology. Scale bars are 5 μm. (b) Quantification of the number of subtraction events observed in control versus exercise cohorts (control 1.68 ± 0.72; exercise 1.32 ± 0.7; $p = 0.73$; $n = 11$ mice, NS $p = 0.73$, Mann-Whitney test). (c) Histogram of all observed capillary segment loop lengths (gray) versus loop lengths of subtracted capillary segments (red). Subtracted loops are members of significantly shorter loops compared to their stable counterparts (166 total loops with shortest loop length 7.24 ± 0.21 segments versus 19 subtracted loops with shortest loop length 5.12 ± 0.5 segments, $n = 12$ mice, ***$p < 0.001$, Mann–Whitney test).

at the offset of running (24 and 48 h after locking the running wheel) and do not find any additional capillary segments that were then removed.

Capillary segment subtractions preferentially prune short vascular loops

Do pre-existing structural features predict the eventual pruning of a capillary segment? We began addressing this question by comparing the length and diameter of to-be-pruned capillary segments with their stable counterparts. Neither the length nor the diameter of subtracted capillaries allowed us to segregate to-be-pruned from stable capillaries ($p > 0.1$, One-sample t-test). In addition, we do not observe a preference for layer, with 60% of the observed subtractions occurring in layer I and 40% in layer II/III.

Next, we asked whether capillary segments that would eventually be pruned were members of particular network topologies. Using the fully reconstructed 3D

vascular network for each imaging volume (see online supplementary methods), we calculated the shortest loop to traverse from each capillary branch point back to itself by counting the number of intervening capillary segments.[7] We find that to-be-pruned segments were members of significantly shorter vascular loops than expected by chance (Figure 6(c); to-be-pruned shortest loop length 5.12 ± 0.5 segments; full network shortest loop length 7.24 ± 0.21 segments; $p < 0.001$ in 12 mice). Interestingly, we occasionally observed loops comprising just two segments (immediate anastomosis) but did not observe any of these loops undergo pruning (online supplementary Figure 7). Thus, capillary segment subtraction does not depend upon the structural parameters of to-be-pruned segments but instead preferentially targets segments with short-loop network topologies.

Capillary pericytes are stable in the adult motor cortex

Although the spatial distribution of pericytes has been described (Figure 2),[40,56] little is known about the temporal dynamics of pericytes. Are pericytes motile or do they remain fixed along their respective capillary segment? Do pericytes undergo ongoing addition and subtraction? To address these questions, we tracked the position of pericyte cell bodies and searched for pericyte cell body addition and subtraction. We tracked a total of 1575 pericytes in eight mice (median of 150 pericytes per animal) and did not see any migratory behavior at short time-scales on the order of a day nor at long time-scales on the order of a month. This indicates that in layers I–III of the adult mouse motor cortex, pericyte cell bodies are non-motile (Figure 7). In addition, we do not see pericyte cell body addition or subtraction. We did, however, observe that a small fraction (12%) of pericyte cell bodies can migrate from one side of a capillary segment to the other, while retaining their position along the capillary length.

Discussion

We have characterized the long-term structural plasticity of cerebral vasculature in the motor cortex of adult mice. In control experiments, we find that the capillary segments throughout cortical layers I–III are remarkably stable both in their structure and network topology. We do not observe capillary segment addition but do see a low level of subtraction that preferentially prunes short vascular loops. We show that pericyte cell bodies are heterogenous in their distribution, targeting a subset of capillary segments with a higher density in cortical layer I versus layer II/III. Pericyte cell bodies are almost entirely non-motile and do not undergo addition and subtraction. Finally, we show that voluntary exercise does not alter any of these structural or dynamic properties of motor cortical vasculature or pericytes.

Pericyte distribution and dynamics in motor cortical layers I–III

The majority of pericyte cell bodies (77%) are positioned en passant along capillary segments with the remaining fraction found as junctional pericytes at capillary branch points (Figure 2). Interestingly, only 43% of capillary segments possess an en passant pericyte cell body. En passant pericyte cell bodies are associated with longer segments and those segments that possess a pericyte cell body are significantly constricted versus their pericyte cell body lacking capillary counterparts. One possibility is that, in basal conditions, the presence of a capillary pericyte may tonically constrict its associated capillary segment, thereby limiting blood flow.

The density of pericyte-bearing capillary segments is higher in cortical layer I versus layer II/III. This layer-specific distribution is in agreement with a recent study that examined the distribution of pericytes using an in vitro cleared-brain preparation and immunohistochemistry.[40] The heterogeneous distribution of pericytes, both among capillary segments and between cortical layers, may endow the capillary network in layers I–III with the ability to precisely control the spatial distribution of blood flow depending on the metabolic demands of the local parenchyma.

In our fixed tissue immunohistochemistry experiments (online supplementary Figure 4), we show that 75% of cells with a GFP bump-on-a-log appearance are co-localized with the pericyte marker CD13 ($GFP^+/CD13^+$). Yet, we do not know the identity of the remaining $GFP^+/CD13^-$ cells. One possibility is they are pericytes that are $CD13^-$ as it has not been shown that this CD13 antibody labels every pericyte. Alternatively, these cells may not be pericytes, despite their sterotyped morphology. Thus, a caveat must be sounded in interpreting our results on the distribution of pericytes between cortical layers (Figure 2) as our *in vivo* analysis of pericytes may include a fraction of other cells and so both endothelial cell and pericyte position may influence capillary diameter, length, and differential cortical layer distribution. Future experiments to further classify these cells are difficult as there is currently no definitive pericyte marker.

Isoflurane anesthetic dilates vessel segments

We find that isoflurane anesthetic dilates all vessel segments in the upper layers of the motor cortex including

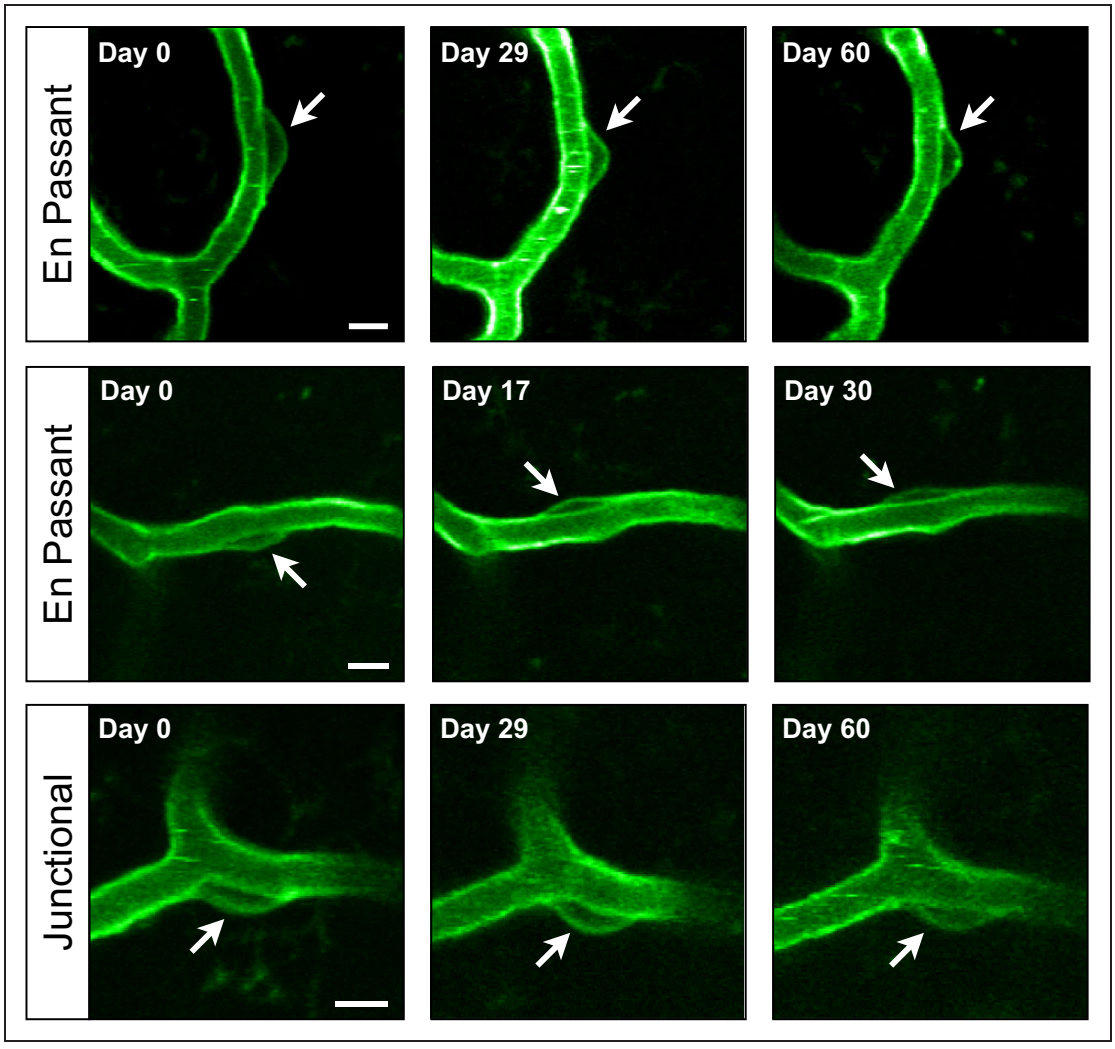

Figure 7. Pericyte cell bodies are stable. Exemplar time-series of individual pericyte cell bodies. Each row is a time-series for a different pericyte cell body with the interval in days shown in the upper left corner of each image. The first row shows a stable en passant pericyte, the second an en passant pericyte that migrates from one side of a capillary segment to the other, and the third shows a stable junctional pericyte. All images are maximal z-projections of two to three imaging planes (4–6 μm). Scale bars are 5 μm.

pial arteries, pial veins, and layer I–III capillary segments (Figure 3). These data provide a positive control for our longitudinal experiments in both baseline (Figure 4) and voluntary exercise (Figure 5) by demonstrating that these vessels are capable of undergoing bidirectional changes in tone.

In addition to dilating cortical vessels,[53] isoflurane is known to increase cerebral blood volume,[57–59] increase capillary Po_2,[54] and decrease arterial blood pressure, yet it has little effect on cerebral blood flow.[52,60,61] While we observe the majority of vessels dilate in response to isoflurane (Figure 3(c)), we see no increase in the volume of the 3D convex hull enclosing the vascular branch points (Figure 3(e)). This may reflect that the brain volume occupied by capillaries vessels is only a portion of total brain volume.

Capillary tone can be influenced by a number of factors both intrinsic and extrinsic to endothelial cells. Intrinsic factors include the activation of K^+ and Ca^{++} channels expressed in endothelial cells.[62] Extrinsic factors include the activation of perivascular nerves,[63] relaxation of precapillary arterial smooth muscle,[64] and the activation of neuronal and astrocytic signaling pathways.[65,66] An additional mechanism for the control of capillary tone is via contractile pericytes.[47] Yet, we do not see a difference in the isoflurane-induced dilatory response of capillaries with and without pericyte cell bodies, suggesting that the locus of effect of isoflurane may be intrinsic to endothelial cells or due to some additional factor such as the dilation of upstream arteries. This is in agreement with a study that found no difference in the dilatory response of capillaries with

and without pericytes in response to cortical spreading depression in the parietal cortex.[36]

Vascular structure is stable in the adult and is not affected by exercise

Through longitudinal imaging of adult mice, we have shown that vascular structure in layers I–III of the motor cortex is stable within individuals as measured by branch point position, vessel segment diameter, and length (Figure 4). We have also shown that pericyte cell bodies are stable; they do not undergo addition or subtraction nor do they migrate along the length of capillary segments. However, sometimes, they can rotate around the axis of a given capillary segment (Figure 7). The stability in both vascular structure and pericytes may reflect very low turnover rates of endothelial cells that can range from months to years (for review, see Brown[67]).

The beneficial neuropsychiatric effects of exercise are far reaching, including the alleviation of anxiety and depression,[30] improved cognitive performance, particularly in later life,[68] and speeding recovery from stroke.[69] While it is well accepted that exercise can induce neuronal structural plasticity, particularly in the hippocampus,[23] the impact of exercise on cerebral vascular structure, and in particular, motor cortical vascular structure has received less attention.

Using fixed tissue toluidine staining, Kleim et al.[21] report that voluntary exercise (~3 km per day for one month) in five-month-old male Long–Evans rats increased the capillary density in layer V of the motor cortex compared to inactive controls. In a similar study with slightly older mixed gender rats (six-month- to one-year-old), Swain et al.[22] used fixed tissue CD61 immunostaining to show that voluntary exercise (~3 km per day for one month) increased capillary density in motor cortical layer II/III but not layer V. The differences between these reports (e.g. increased density in layer V versus no increase) could be due to differences in age, gender, or in the staining protocol used. A fixed tissue study in the cynomolgus monkey by Rhyu et al.[71] found that voluntary exercise (~3 km per day for five months) increased capillary density through all layers of the motor cortex in older (15–17 years old) but not middle-aged (10–12 years old) monkeys. The mice we used in the present study (three to six months of age) correspond to the mature adult and are younger than middle-aged.[70] Thus, our results are in agreement with Rhyu et al.[71] One potential explanation to reconcile these various results is that voluntary exercise may have more of an effect on the aged versus younger motor cortex.

The previous studies that assessed vascular density in the motor cortex with exercise[21,22,71] utilized population averaging in fixed-tissue slice preparations and thus could be missing potentially important *in vivo* 3D measurements. In particular, they lack the ability to track the temporal evolution of vascular density within individual animals. However, one advantage of fixed tissue studies is the ability to survey much larger volumes of brain tissue than can be monitored with *in vivo* two-photon imaging.

Here, we show that voluntary exercise does not induce the sprouting or regression of capillary segments in the upper layer of the motor cortex within individual mice. If voluntary exercise were to increase capillary density, we would have seen this as the addition of vascular segments within individuals. The vascular stability we find is striking given our mice can run in excess of 10–12 km per day, each day, for upwards of one month. This vascular stability is in contrast to experiments showing that voluntary exercise in humans can induce vascular sprouting in skeletal muscle[72,73] that can even impact non-activated muscles.[74]

Exercise is a complex behavior and, thus, could also act as a form of sensory enrichment and motor learning. Both sensory enrichment[75] and motor learning[76,77] are known to induce rewiring of neuronal circuits. Thus, we were surprised to find that exercise does not also impart changes in vascular structure. One possibility is that already established vascular networks are sufficient to accommodate changes in the metabolic demand of brain parenchyma produced in response to voluntary exercise.

It may be that exercise has a more pronounced effect on the real-time dynamics of cerebral vasculature that would result in alterations in blood flow. For example, in humans, movement evoked blood flow is increased following periods of exercise.[78] Another possibility is that exercise could induce vascular plasticity when the vasculature is compromised in disease. For example, exercise could exert an influence on pathological vasculature in diabetes,[79–81] vascular dementia and Alzheimer's disease,[82] and following a stroke.[33] Furthermore, if the vascular and pericyte stability we observe is disrupted, this could contribute to the etiology and pathology of disease. For example, pericyte loss precedes diabetic retinopathy[83] and is associated with accelerated progression of Alzheimer's disease pathogenesis.[46,84]

The motor cortex undergoes a slow rate of vessel subtraction

We observe a low rate of vessel segment subtraction that is not counterbalanced by addition of vessel segments. These rare vessel subtraction events in the adult do not proceed randomly but preferentially prune short vascular loops (Figure 6). We do not know the mechanism by which this occurs. One possibility is that short loops have reduced or turbulent flow and reductions in

sheer stress, which are known to act as a trigger for vessel pruning.[85] The pruning of short vascular loops was first observed in the tail of developing frog larva.[86] More recently, short-loop pruning in the brain of embryonic zebrafish has been proposed as a process that makes vascular network topology more efficient.[87] One possibility is that these pruning events could represent a house-keeping mechanism to improve the efficiency of blood delivery to the parenchyma by removing redundant or ineffective network topologies.

Vascular pruning events observed herein (Figure 6) resemble 'string vessels' which are the remnants of previously pruned capillary segments that have been observed in fixed brain tissue.[67,88] Our time-lapse images of pruning events share striking resemblance to pruning events described in the early postnatal mouse retina[89] and the digestive tract of larval zebrafish.[90] Summed over the lifespan, this rare process (approximately 0.16 subtractions per day per mm^3) could contribute to reduced cortical vascular density seen in aged animals[91] and potentially contribute to a host of age-related pathologies including cognitive decline and vascular dementia,[92] the general susceptibility of the aged brain to the incidence of stroke[93] and, perhaps, the increased severity of damage in response to traumatic brain injury.[94]

Funding

The author(s) disclosed receipt of the following financial support for the research, authorship, and/or publication of this article: We thank the Brain Sciences Institute of Johns Hopkins University for pilot grant support. RHC was supported by an AHA SDG grant (16SDG27130006) and SED was supported by an NIH F32 grant (NS090822). Immunohistological imaging was performed in the Johns Hopkins Imaging Core Facility (NIH NS050274).

Acknowledgements

We thank Jeremy Nathans and Ray Koehler for feedback on experimental design. Thanks to Ethan Hughes, Amit Agarwal, Steven Zeiler, and member of Linden lab for helpful discussions and Jeremy Nathans and Andrew Ewald for gifts of mTmG and Tie2-Cre mice. Special thanks to Jeremy Nathans for initially suggesting the utility of using the Tie2-Cre:mTmG cross to visualize vasculature in adult mice. Thanks to Terry Shelley for machining microscope parts (NINDS Core Center Grant, P30 NS050274). Finally, we would like to thank our hardworking undergraduate image analysts Jahnavi Cruz Diaz, Sam Eberlein, Clarissa Martin, and Christopher Micek.

Declaration of Conflicting Interests

The author(s) declared no potential conflicts of interest with respect to the research, authorship, and/or publication of this article.

Authors' contributions

RHC and DJL conceived experiments. RHC performed all cranial window surgeries, *in vivo* imaging, wrote analytical software, and conducted the analysis. SED performed the immunohistochemistry. RHC and DJL wrote the manuscript.

Supplementary material

Supplementary material for this paper can be found at http://journals.sagepub.com/doi/suppl/10.1177/0271678X16682508

References

1. Attwell D and Laughlin SB. An energy budget for signaling in the grey matter of the brain. *J Cereb Blood Flow Metab* 2001; 21: 1133–1145.
2. Vazquez AL, Masamoto K, Fukuda M, et al. Cerebral oxygen delivery and consumption during evoked neural activity. *Front Neuroenerget* 2010; 2: 11.
3. Girouard H and Iadecola C. Neurovascular coupling in the normal brain and in hypertension, stroke, and Alzheimer disease. *J Appl Physiol* 2006; 100: 328–335.
4. Lecrux C and Hamel E. The neurovascular unit in brain function and disease. *Acta Physiol* 2011; 203: 47–59.
5. Attwell D and Iadecola C. The neural basis of functional brain imaging signals. *Trends Neurosci* 2002; 25: 621–625.
6. Hillman EMC. Coupling mechanism and significance of the BOLD signal: a status report. *Annu Rev Neurosci* 2014; 37: 161–181.
7. Blinder P, Tsai PS, Kaufhold JP, et al. The cortical angiome: an interconnected vascular network with noncolumnar patterns of blood flow. *Nat Neurosci* 2013; 16: 889–897.
8. Adams RH and Alitalo K. Molecular regulation of angiogenesis and lymphangiogenesis. *Nat Rev Mol Cell Biol* 2007; 8: 464–478.
9. Herbert SP and Stainier DYR. Molecular control of endothelial cell behaviour during blood vessel morphogenesis. *Nat Rev Mol Cell Biol* 2011; 12: 551–564.
10. Boero JA, Ascher J, Arregui A, et al. Increased brain capillaries in chronic hypoxia. *J Appl Physiol* 1999; 86: 1211–1219.
11. Harb R, Whiteus C, Freitas C, et al. *In vivo* imaging of cerebral microvascular plasticity from birth to death. *J Cereb blood flow Metab* 2013; 33: 146–156.
12. Andreone BJ, Lacoste B and Gu C. Neuronal and vascular interactions. *Annu Rev Neurosci* 2014; 38: 150317183158003.
13. Lacoste B, Comin CH, Ben-Zvi A, et al. Sensory-related neural activity regulates the structure of vascular networks in the cerebral cortex. *Neuron* 2014; 83: 1117–1130.
14. Whiteus C, Freitas C and Grutzendler J. Perturbed neural activity disrupts cerebral angiogenesis during a postnatal critical period. *Nature* 2014; 505: 407–411.
15. Lacoste B and Gu C. Control of cerebrovascular patterning by neural activity during postnatal development. *Mech Dev*. Epub ahead of print 24 June 2015. DOI: 10.1016/j.mod.2015.06.003.

16. Masamoto K, Takuwa H, Seki C, et al. Microvascular sprouting, extension, and creation of new capillary connections with adaptation of the neighboring astrocytes in adult mouse cortex under chronic hypoxia. *J Cereb Blood Flow Metab* 2014; 34: 325–331.
17. Harrison TC, Ayling OGS and Murphy TH. Distinct cortical circuit mechanisms for complex forelimb movement and motor map topography. *Neuron* 2012; 74: 397–409.
18. Berggren KL, Kay JJM and Swain RA. Examining cerebral angiogenesis in response to physical exercise. *Methods Mol Biol* 2014; 1135: 139–154.
19. Black JE, Isaacs KR, Anderson BJ, et al. Learning causes synaptogenesis, whereas motor activity causes angiogenesis, in cerebellar cortex of adult rats. *Proc Natl Acad Sci U S A* 1990; 87: 5568–5572.
20. Isaacs KR, Anderson BJ, Alcantara AA, et al. Exercise and the brain: angiogenesis in the adult rat cerebellum after vigorous physical activity and motor skill learning. *J Cereb Blood Flow Metab* 1992; 12: 110–119.
21. Kleim JA, Cooper NR and VandenBerg PM. Exercise induces angiogenesis but does not alter movement representations within rat motor cortex. *Brain Res* 2002; 934: 1–6.
22. Swain RA, Harris AB, Wiener EC, et al. Prolonged exercise induces angiogenesis and increases cerebral blood volume in primary motor cortex of the rat. *Neuroscience* 2003; 117: 1037–1046.
23. van Praag H, Shubert T, Zhao C, et al. Exercise enhances learning and hippocampal neurogenesis in aged mice. *J Neurosci* 2005; 25: 8680–8685.
24. Ding Y-H, Li J, Zhou Y, et al. Cerebral angiogenesis and expression of angiogenic factors in aging rats after exercise. *Curr Neurovasc Res* 2006; 3: 15–23.
25. Dombeck DA, Graziano MS and Tank DW. Functional clustering of neurons in motor cortex determined by cellular resolution imaging in awake behaving mice. *J Neurosci* 2009; 29: 13751–13760.
26. Motoike T, Loughna S, Perens E, et al. Universal GFP reporter for the study of vascular development. *Genesis* 2000; 28: 75–81.
27. Villringer A, Them A, Lindauer U, et al. Capillary perfusion of the rat brain cortex: an *in vivo* confocal microscopy study. *Circ Res* 1994; 75: 55–62.
28. Kleinfeld D, Mitra PP, Helmchen F, et al. Fluctuations and stimulus-induced changes in blood flow observed in individual capillaries in layers 2 through 4 of rat neocortex. *Proc Natl Acad Sci U S A* 1998; 95: 15741–15746.
29. Kisanuki YY, Hammer RE, Miyazaki J, et al. Tie2-Cre transgenic mice: a new model for endothelial cell-lineage analysis *in vivo*. *Dev Biol* 2001; 230: 230–242.
30. Carek PJ, Laibstain SE and Carek SM. Exercise for the treatment of depression and anxiety. *Int J Psychiatry Med* 2011; 41: 15–28.
31. Colcombe SJ, Kramer AF, Erickson KI, et al. Cardiovascular fitness, cortical plasticity, and aging. *Proc Natl Acad Sci U S A* 2004; 101: 3316–3321.
32. van Praag H. Exercise and the brain: something to chew on. *Trends Neurosci* 2009; 32: 283–290.
33. Murphy TH and Corbett D. Plasticity during stroke recovery: from synapse to behaviour. *Nat Rev Neurosci* 2009; 10: 861–872.
34. Muzumdar MD, Tasic B, Miyamichi K, et al. A global double-fluorescent Cre reporter mouse. *Genesis* 2007; 45: 593–605.
35. Hill RA, Tong L, Yuan P, et al. Regional blood flow in the normal and ischemic brain is controlled by arteriolar smooth muscle cell contractility and not by capillary pericytes. *Neuron* 2015; 87: 95–110.
36. Fernández-Klett F, Offenhauser N, Dirnagl U, et al. Pericytes in capillaries are contractile *in vivo*, but arterioles mediate functional hyperemia in the mouse brain. *Proc Natl Acad Sci U S A* 2010; 107: 22290–22295.
37. Mishra A, O'Farrell FM, Reynell C, et al. Imaging pericytes and capillary diameter in brain slices and isolated retinae. *Nat Protoc* 2014; 9: 323–336.
38. Iurlaro M, Scatena M, Zhu W-H, et al. Rat aorta-derived mural precursor cells express the Tie2 receptor and respond directly to stimulation by angiopoietins. *J Cell Sci* 2003; 116: 3635–3643.
39. De Palma M, Venneri MA, Galli R, et al. Tie2 identifies a hematopoietic lineage of proangiogenic monocytes required for tumor vessel formation and a mesenchymal population of pericyte progenitors. *Cancer Cell* 2005; 8: 211–26.
40. Hartmann DA, Underly RG, Watson AN, et al. A murine toolbox for imaging the neurovascular unit. *Microcirculation* 2015; 22: 168–182.
41. Narayanaswamy A, Dwarakapuram S, Bjornsson CS, et al. Robust adaptive 3-D segmentation of vessel laminae from fluorescence confocal microscope images and parallel GPU implementation. *IEEE Trans Med Imaging* 2010; 29: 583–97.
42. Ukwatta E, Yuan J, Qiu W, et al. Joint segmentation of lumen and outer wall from femoral artery MR images: towards 3D imaging measurements of peripheral arterial disease. *Med Image Anal* 2015; 26: 120–132.
43. Peppiatt CM, Howarth C, Mobbs P, et al. Bidirectional control of CNS capillary diameter by pericytes. *Nature* 2006; 443: 700–704.
44. Bell RD, Winkler EA, Sagare AP, et al. Pericytes control key neurovascular functions and neuronal phenotype in the adult brain and during brain aging. *Neuron* 2010; 68: 409–427.
45. Mathiisen TM, Lehre KP, Danbolt NC, et al. The perivascular astroglial sheath provides a complete covering of the brain microvessels: an electron microscopic 3D reconstruction. *Glia* 2010; 58: 1094–103.
46. Sagare AP, Bell RD, Zhao Z, et al. Pericyte loss influences Alzheimer-like neurodegeneration in mice. *Nat Commun* 2013; 4: 2932.
47. Hall CN, Reynell C, Gesslein B, et al. Capillary pericytes regulate cerebral blood flow in health and disease. *Nature* 2014; 508: 55–60.

48. Fernández-Klett F and Priller J. Diverse functions of pericytes in cerebral blood flow regulation and ischemia. *J Cereb Blood Flow Metab* 2015; 35: 883–887.
49. Sweeney MD, Ayyadurai S and Zlokovic BV. Pericytes of the neurovascular unit: key functions and signaling pathways. *Nat Neurosci* 2016; 19: 771–783.
50. Flynn NM, Buljubasic N, Bosnjak ZJ, et al. Isoflurane produces endothelium-independent relaxation in canine middle cerebral arteries. *Anesthesiology* 1992; 76: 461–467.
51. Koenig HM, Pelligrino DA, Wang Q, et al. Role of nitric oxide and endothelium in rat pial vessel dilation response to isoflurane. *Anesth Analg* 1994; 79: 886–891.
52. Masamoto K, Fukuda M, Vazquez A, et al. Dose-dependent effect of isoflurane on neurovascular coupling in rat cerebral cortex. *Eur J Neurosci* 2009; 30: 242–250.
53. Gao YR, Greene SE and Drew PJ. Mechanical restriction of intracortical vessel dilation by brain tissue sculpts the hemodynamic response. *Neuroimage* 2015; 115: 162–176.
54. Lyons DG, Parpaleix A, Roche M, et al. Mapping oxygen concentration in the awake mouse brain. *Elife*. Epub ahead of print 2 Febrauary 2016. DOI: 10.7554/eLife.12024.
55. Van der Borght K, Kóbor-Nyakas DE, Klauke K, et al. Physical exercise leads to rapid adaptations in hippocampal vasculature: temporal dynamics and relationship to cell proliferation and neurogenesis. *Hippocampus* 2009; 19: 928–936.
56. Ghosh M, Balbi M, Hellal F, et al. Pericytes are involved in the pathogenesis of cerebral autosomal dominant arteriopathy with subcortical infarcts and leukoencephalopathy. *Ann Neurol* 2015; 78: 887–900.
57. Archer DP, Labrecque P, Tyler JL, et al. Cerebral blood volume is increased in dogs during administration of nitrous oxide or isoflurane. *Anesthesiology* 1987; 67: 642–648.
58. Weeks JB, Todd MM, Warner DS, et al. The influence of halothane, isoflurane, and pentobarbital on cerebral plasma volume in hypocapnic and normocapnic rats. *Anesthesiology* 1990; 73: 461–466.
59. Kim T, Hendrich KS, Masamoto K, et al. Arterial versus total blood volume changes during neural activity-induced cerebral blood flow change: implication for BOLD fMRI. *J Cereb Blood Flow Metab* 2007; 27: 1235–1247.
60. Scheller MS, Tateishi A, Drummond JC, et al. The effects of sevoflurane on cerebral blood flow, cerebral metabolic rate for oxygen, intracranial pressure, and the electroencephalogram are similar to those of isoflurane in the rabbit. *Anesthesiology* 1988; 68: 548–551.
61. Masamoto K and Kanno I. Anesthesia and the quantitative evaluation of neurovascular coupling. *J Cereb Blood Flow Metab* 2012; 32: 1233–1247.
62. Longden TA, Hill-Eubanks DC and Nelson MT. Ion channel networks in the control of cerebral blood flow. *J Cereb Blood Flow Metab* 2016; 36: 492–512.
63. Hamel E. Perivascular nerves and the regulation of cerebrovascular tone. *J Appl Physiol* 2006; 100: 1059–1064.
64. Davis MJ. Perspective: physiological role(s) of the vascular myogenic response. *Microcirculation* 2012; 19: 99–114.
65. Iadecola C and Nedergaard M. Glial regulation of the cerebral microvasculature. *Nat Neurosci* 2007; 10: 1369–1376.
66. Attwell D, Buchan AM, Charpak S, et al. Glial and neuronal control of brain blood flow. *Nature* 2010; 468: 232–43.
67. Brown WR. A review of string vessels or collapsed, empty basement membrane tubes. *J Alzheimers Dis* 2010; 21: 725–739.
68. Ratey JJ and Loehr JE. The positive impact of physical activity on cognition during adulthood: a review of underlying mechanisms, evidence and recommendations. *Rev Neurosci* 2011; 22: 171–185.
69. Krakauer JW, Carmichael ST, Corbett D, et al. Getting neurorehabilitation right: what can be learned from animal models? *Neurorehabil Neural Repair* 2012; 26: 923–931.
70. Flurkey K, Currer JM and Harrison DE. Mouse models in aging research. In: Fox JG, Davisson MT, Quimby FW, et al. (eds) *The Mouse in Biomedical Research*. Amsterdam: Elsevier, 2007, pp.637–672.
71. Rhyu IJ, Bytheway JA, Kohler SJ, et al. Effects of aerobic exercise training on cognitive function and cortical vascularity in monkeys. *Neuroscience* 2010; 167: 1239–1248.
72. Prior BM, Yang HT and Terjung RL. What makes vessels grow with exercise training? *J Appl Physiol* 2004; 97: 1119–1128.
73. Laughlin MH and Roseguini B. Mechanisms for exercise training-induced increases in skeletal muscle blood flow capacity: differences with interval sprint training versus aerobic endurance training. *J Physiol Pharmacol* 2008; 59(Suppl. 7): 71–88.
74. Padilla J, Simmons GH, Bender SB, et al. Vascular effects of exercise: endothelial adaptations beyond active muscle beds. *Physiology* 2011; 26: 132–145.
75. Feldman DE and Brecht M. Map plasticity in somatosensory cortex. *Science* 2005; 310: 810–815.
76. Yang G, Pan F and Gan W-B. Stably maintained dendritic spines are associated with lifelong memories. *Nature* 2009; 462: 920–924.
77. Fu M, Yu X, Lu J, et al. Repetitive motor learning induces coordinated formation of clustered dendritic spines *in vivo*. *Nature* 2012; 483: 92–95.
78. Bullitt E, Rahman FN, Smith JK, et al. The effect of exercise on the cerebral vasculature of healthy aged subjects as visualized by MR angiography. *Am J Neuroradiol* 2009; 30: 1857–1863.
79. Li W, Prakash R, Kelly-Cobbs AI, et al. Adaptive cerebral neovascularization in a model of type 2 diabetes: relevance to focal cerebral ischemia. *Diabetes* 2010; 59: 228–235.
80. Prakash R, Somanath PR, El-Remessy AB, et al. Enhanced cerebral but not peripheral angiogenesis in the Goto-Kakizaki model of type 2 diabetes involves VEGF and peroxynitrite signaling. *Diabetes* 2012; 61: 1533–1542.

81. Prakash R, Johnson M, Fagan SC, et al. Cerebral neovascularization and remodeling patterns in two different models of type 2 diabetes. *PLoS One* 2013; 8: e56264.
82. Farkas E and Luiten PG. Cerebral microvascular pathology in aging and Alzheimer's disease. *Prog Neurobiol* 2001; 64: 575–611.
83. Beltramo E and Porta M. Pericyte loss in diabetic retinopathy: mechanisms and consequences. *Curr Med Chem* 2013; 20: 3218–3225.
84. Halliday MR, Rege SV, Ma Q, et al. Accelerated pericyte degeneration and blood-brain barrier breakdown in apolipoprotein E4 carriers with Alzheimer's disease. *J Cereb Blood Flow Metab* 2016; 36: 216–227.
85. Korn C and Augustin HG. Mechanisms of vessel pruning and regression. *Dev Cell* 2015; 34: 5–17.
86. Clark ER. Studies on the growth of blood-vessels in the tail of the frog larva – by observation and experiment on the living animal. *Am J Anat* 1918; 23: 37–88.
87. Chen Q, Jiang L, Li C, et al. Haemodynamics-driven developmental pruning of brain vasculature in zebrafish. *PLoS Biol* 2012; 10: e1001374.
88. Brown WR and Thore CR. Review: cerebral microvascular pathology in ageing and neurodegeneration. *Neuropathol Appl Neurobiol* 2011; 37: 56–74.
89. Franco CA, Jones ML, Bernabeu MO, et al. Dynamic endothelial cell rearrangements drive developmental vessel regression. *PLoS Biol* 2015; 13: e1002125.
90. Lenard A, Daetwyler S, Betz C, et al. Endothelial cell self-fusion during vascular pruning. *PLoS Biol* 2015; 13: e1002126.
91. Janota C, Lemere CA and Brito MA. Dissecting the contribution of vascular alterations and aging to Alzheimer's disease. *Mol Neurobiol* 2016; 53: 3793–3811.
92. Stephan BCM and Brayne C. Vascular factors and prevention of dementia. *Int Rev Psychiatry* 2008; 20: 344–356.
93. Popa-Wagner A, Carmichael ST, Kokaia Z, et al. The response of the aged brain to stroke: too much, too soon? *Curr Neurovasc Res* 2007; 4: 216–227.
94. Bruns J and Hauser WA. The epidemiology of traumatic brain injury: a review. *Epilepsia* 2003; 44: 2–10.